Composite Structures 123 (2015) 204–215

Contents lists available at ScienceDirect

Composite Structures

journal homepage: www.elsevier.com/locate/compstruct

Behaviour of corroded shear-critical reinforced concrete beams repaired with NSM CFRP rods

Belal Almassri [a], Amjad Kreit [a], Firas Al Mahmoud [b], Raoul Francois [a,*]

[a] Université de Toulouse, UPS, INSA, LMDC (Laboratoire Matériaux et Durabilité des Constructions), Toulouse, France
[b] Institut Jean Lamour, UMR 7198, CNRS, Université de Lorraine, Nancy, France

ARTICLE INFO

Article history:
Available online 30 December 2014

Keywords:
Carbon fibre reinforced polymers
Reinforced concrete
Corrosion
Shear strengthening
Shear failure
Near surface mounted (NSM)

ABSTRACT

This paper discusses the results of an experimental program designed to investigate the effect of repairing the RC corroded shear-critical deep beams with near surface mounted (NSM) carbon fibre-reinforced polymer (CFRP) rods. A 28-year-old RC beam corroded by exposure to a chloride environment was cut into two small short-shear-span beams, along with a control beam of the same characteristics (age, length and cross-section). One RC corroded deep beam was repaired in bending and the other one was repaired in both bending and shear with NSM CFRP rods. Force–displacement curves were plotted for the corroded and control beams. After the beams had been tested up to failure, the loss of mass was measured and plotted for both the longitudinal and transverse reinforcement. The slip of tensile reinforcement at the end of the beams was also measured during the tests.

Experimental results show that both corroded and control deep beams repaired only in bending failed due to shear mode of failure (diagonal tension failure), while corroded and control beams repaired in both bending and shear failed due to concrete crushing. The test results also showed that the corrosion of both longitudinal and transversal reinforcement hardly modified the mechanical response of deep beams.

1. Introduction

The cost of rehabilitating corroded RC structures worldwide exceeds $1.8 trillion per year [1]. Corrosion of the steel bars in the RC elements causes a reduction in the cross sectional area of the steel reinforcement and a significant reduction in its ductility, which leads to the early failure of steel bars [2,3]. Most of the experimental research literature mainly focuses on the effect of steel corrosion on the flexural behaviour of reinforced concrete elements [4–7] and, so far, little research has concerned the effect of corrosion on the shear behaviour of corroded reinforced concrete beams. Accelerated corrosion tests were conducted on RC beams [8–10] in order to understand the effect of the corroded steel stirrups on the shear behaviour of RC beams. Instead of using impressed current induced corrosion, some studies [11,12] have aimed to assess the shear behaviour of naturally corroded RC beams. This work was based on a long-term programme in which the RC beams were stored in a chloride environment under service loads in order to obtain results that were closer to the real state of corroded structures.

The near surface mounted reinforcement technique (NSM) using carbon fibre reinforced polymer (CFRP) rods is a strengthening technique that has given encouraging results in repairing deteriorated RC beams that are likely to fail in a brittle shear failure mode. De Lorenzis and Nanni, [13] showed that the use of NSM FRP rods could improve the shear capacity of RC beams, a 106% increase in the shear strength being recorded in the absence of internal steel stirrups. A significant increase was also recorded for limited shear reinforced beams. Islam [14] tested four concrete beams: a control beam having typical shear steel reinforcement and three other beams that were strengthened in shear with CFRP bars using the NSM technique, for which a 17–25% increase in shear strength was found.

Rizzo and De Lorenzis, [15] carried out a testing program in order to assess the shear capacity increase that could be obtained by using the NSM FRP reinforcement technique, and made a comparison between the externally bonded U-wrapped laminates and the NSM technique. One side of each beam was reinforced strongly in shear with 10 mm diameter stirrups every 50 mm, while the other side was reinforced with a limited shear reinforcement using 6 mm diameter stirrups every 160 mm. The beams were simply supported and were tested with a four-point loading test. The beams strengthened with the NSM technique, both NSM round

* Corresponding author.

http://dx.doi.org/10.1016/j.compstruct.2014.12.043
0263-8223/

bars and NSM strips were used, an increase in the shear capacity of 16% was recorded for the beam strengthened with externally bonded U-wrapped laminate, while 45 degrees inclination of beams strengthened with NSM round bars and NSM strips gave 14% and 9.4% increase in the shear capacity over using the 90 degrees of U-wrapped laminate as strengthening technique respectively. Dias and Barros, [16] also found that the NSM technique using CFRP laminates had advantages over the externally bonded reinforcement (EBR) technique in terms of maximum load-bearing capacity and load capacity after shear crack formation, and found much higher strain values in the CFRP rods, which means that the NSM technique makes better use of the tensile strength of the CFRP material.

De Lorenzis et al. [17] suggested some methods for increasing the shear capacity of the strengthened T-beams by decreasing the space between the FRP rods and increasing the anchorage length of the FRP rods in a T-beam that was also anchored to the flange. They mentioned that decreasing the space between the FRP rods which corresponds to an increase in the FRP material inside the RC beam will lead to an important increase in the shear capacity of the RC beam. They also mentioned that inclining the FRP rods at 45 degrees increased the shear capacity of the reinforced concrete elements, in agreement with the findings of Barros et al. [18] on inclined FRP laminates, which proved to be more effective than vertical laminates.

De Lorenzis and Nanni [13] observed two failure modes for beams repaired in shear with NSM FRP rods. The first was de-bonding of the FRP rods and the second was splitting of the concrete cover over the longitudinal steel bars. They concluded that, once failure by FRP rod de-bonding was prevented by using inclined rods rather than vertical ones, splitting of the concrete cover of the longitudinal steel reinforcement was the most important factor controlling the mode of failure. Another failure mode observed [15] was the splitting of the concrete cover side of all of the internal steel stirrups.

The present paper studies the post-repair performance of corroded short-span reinforced concrete beams repaired with the NSM FRP technique. Some of these beams were repaired in bending only and the others were repaired in bending and shear. All were tested statically in three-point loading up to failure. The failure modes and the mechanical performance of all beams were studied, and the shear capacity of the short-span corroded beams repaired in shear and bending was compared to that of similar non-repaired beams. The relationship between the shear strength of the RC beam and its span to section depth ratio was also studied and the slipping of the steel bars was measured for all beams during the loading tests. Finally, the corroded steel bars were extracted from the beams to study their corrosion and tensile tests were conducted to study their mechanical properties.

2. Experimental program: specimens, test setup, monitoring system and material properties

2.1. Experimental procedure

An experimental programme was started at LMDC (Laboratory of Materials and Durability of Constructions) in 1984 with the aim of understanding the effects of steel corrosion on the structural behaviour of RC elements. This long-term programme consisted of casting a set of 72 RC beams of dimensions 3000 × 280 × 150 mm. Thirty-six of them were stored in a chloride environment under service load to measure the flexural cracks occurring during the corrosion process. Many experimental studies have been conducted on these beams to evaluate the development of corrosion cracking, to measure chloride content and to analyse the changes in their mechanical behaviour [19,20]. The other 36 beams were stored under the same mechanical load but in a non-aggressive environment to be used later as control beams in the study of long-term effects, such as creep and ageing of the concrete. The natural aggressive environment system consisted of salt fog spray (35 g/l of NaCl) (see Fig. 1).

For 9 years, the beams were under sustained loadings in chloride environment in the laboratory conditions so the temperature was controlled (around 20 °C) while after 9 years the salt fog chamber was transferred outside so the temperature was not controlled and the beams were exposed to the outside temperature with monthly-average values ranging from 5.1 °C to 21.3 °C. The beams have been stored in the saline fog for 6 years; the corroded beams were transferred to wetting–drying cycles in order to accelerate the corrosion process (Table 1). The loading system was allowed to monitor the decrease of the force applied due to concrete creep, and then the load was re-adjusted periodically during the first years. Moreover, a spring system of the loading device was allowed to accept some increase in beam deflection without affecting the load. Nevertheless, the loading device was kept in the aggressive environment and the monitoring system stopped giving load information after 6 years. After 19 years of storage, it was decided to perform mechanical tests on the beams, the loading system was removed. However, because of the high chloride content [21] and storage conditions, corrosion continued to propagate.

The corrosion obtained in this climate-accelerated programme was very close to the corrosion observed under natural conditions in terms of corrosion distribution, corrosion type and oxides produced. The corrosion distribution was largely stochastic with a maximum corrosion pit to average corrosion ratio between 4 and 8. The hydroxyl-oxides played a significant role in the corrosion products. While for the three forms of the hydroxyl-oxides, Geothite was in considerable proportion, and then followed by Akaganeite. Lepidocrocite was relatively weaker. The content of Lepidocrocite was still higher than Magnetite [22,23]. To predict the service life of RC elements, it is very important to have access to such natural degradation [24] rather than that resulting from the use of an applied current or a $CaCl_2$ admixture in the concrete [25,26]. The beams were divided into two groups named type A and type B, which had different reinforcement layouts but the same reinforcing steel bar (yield strength = 500 MPa). Beams A and B had 40 mm and 10 mm of concrete cover respectively. According to French standards at the time of manufacturing [27], the 40 mm cover represents the minimum concrete cover in very aggressive environments (i.e. chloride aggression) and the 10 mm cover represents the minimum concrete cover in a non-aggressive environment. The beams were loaded in three-point flexure by

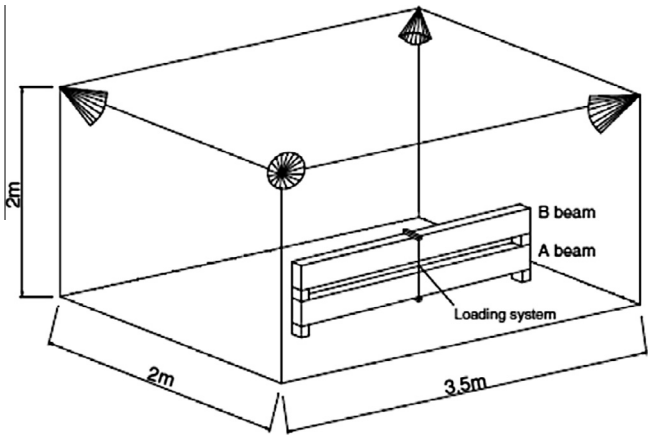

Fig. 1. The climate accelerated aggressive environment system.

Table 1
Wetting–drying cycles of the corroded beams.

Years	Spraying state	Loading conditions	Conservation conditions	Temperature
0–6	Continuous	Loaded	Confined room	20 °C
6–9	WDC*	Loaded	Confined room	20 °C
9–19	WDC*	Loaded	Open room	CSWF**
19–27	Stopped	Unloaded	Open room	CSWF**
27-present	WDC*	Unloaded	Open room	CSWF**

* WDC: wetting–drying cycles for one week respectively.
** CSWF: climate of south–west of France, ranging from 5.1 to 21.3 °C average value per month.

coupling a type A beam with a type B beam. Two loading values were applied: Mser1 = 13.5 kN m for beams referred to as A1 (A1CL3-R and A1T-R); The loading value for type A2 beam was designed according to ultimate load limit state (ULS) in a non-aggressive environment while the loading value for type A1 beam was designed according to serviceability limit state (SLS) requirements for steel corrosion in an aggressive chloride environment based on an indirect limitation of crack width using a tensile stress limitations of the steel bars [27]. Mser2 = 21 kN m for beams referred to as A2 (A2CL1, A2CL3, A2T and A2TI), which had the same type and shape of reinforcement but different values of service loading. The beams studied in this paper are type A beams; one corroded beam (A1CL3-R) and one control beam (A1T-R). Long-term corroded beams A2CL1, A2CL3, A2TI and A2T tested by [21,28] but not repaired were also used here for comparison. The control beam A1T-R was strengthened using the same method as the one used to repair the corroded beam A1CL3-R. The layout of the reinforcement is shown in Fig. 2. The flexural and shear reinforcement ratios were equal to 1.2% and 0.2% respectively. Flexural reinforcement ratio of 1.2% refers to an under reinforced beams state as for this case it is guaranteed that the crushing of concrete will not be reached "earlier" at smaller deformations. Fig. 2 shows the steel distribution inside type A beams.

2.2. Material properties

2.2.1. Concrete properties

The concrete mix is given in Table 2. The Water/Cement ratio was 0.5 but could be adjusted by changing the water quantity to obtain a constant workability of 7 cm in the slump test (slump class S2) in order to meet the most commonly specified consistence according to European Standard EN 206-1 [29]. The average compressive strength and the elastic modulus obtained according to European Standard NF EN 12390-2 [30] on three cylindrical specimens (diameter 11 cm × height 22 cm) tested after 28 days were 45 MPa and 32 GPa respectively. The tensile strength, measured using the splitting test, was 4.7 MPa. Water porosity was 15.2% according to [31]. To measure concrete characteristics, cylindrical cores 70 mm × 140 mm, were drilled out of both the corroded and control beams and tested in compression. Table 3 gives the results of these core tests.

Table 2
Concrete mix.

Mix component	mm	kg/m^3
Rolled gravel (silica + limestone)	5/15	1220
Sand	0/5	820
Portland cement: OPC HP		400
Water		200

Table 3
Mechanical characteristics of the concrete at 27 years (average of 3 tests).

Mechanical characteristics	A1CL3-R	A1T-R
Compressive strength (MPa)	62.2	58.9
Elastic modulus (MPa)	33,700	29,700

Table 4
Effective mechanical properties of steel bars (calculated from the residual cross-section).

Specimen type	Yield strength (MPa)	Ultimate strength (MPa)	Yield strain (%)	Elastic modulus (GPa)
Corroded	578	710	0.27	200
Non-corroded	600	645	0.28	214

2.2.2. Characteristics of steel bars, CFRP bars and filling material

The steel reinforcing bars were composed of natural S500 half-hard steels and were ordinary ribbed bars. The steel bar characteristics were measured after extracting the corroded bars from the corroded beam A1CL3-R and the results are shown in Table 4.

Al-Mahmoud et al. [32] measured the mechanical properties of CFRP rods through a test programme conducted on 3 specimens tested in axial tension. The CFRP rods showed brittle failure that started with splitting and ended with the failure of the rods as shown in Fig. 3. Table 5 shows the mechanical properties of the CFRP rods. In order to increase the bonding between the CFRP rods and the filling material, the rods were coated with 0.2/0.3 mm of surface sanding material, which was sprinkled onto an epoxy paste applied to the surface of the rods.

Table 6 shows the characteristics of the filling material (epoxy paste) after 7 days according to the manufacturer's specifications.

2.3. Repair technique with NSM against bending and shear forces

The NSM CFRP rod was installed in the corroded beam A1CL3-R and in the control beam A1T-R by making two cuts in the concrete cover in the longitudinal direction at the tension side. A special concrete saw with a diamond blade was used.

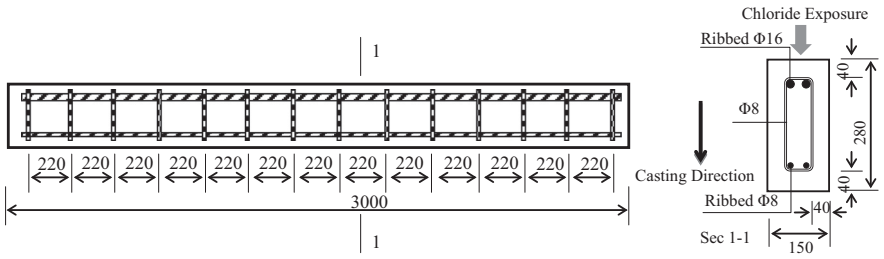

Fig. 2. Reinforcement layout of type A beams. Dimensions are in mm.

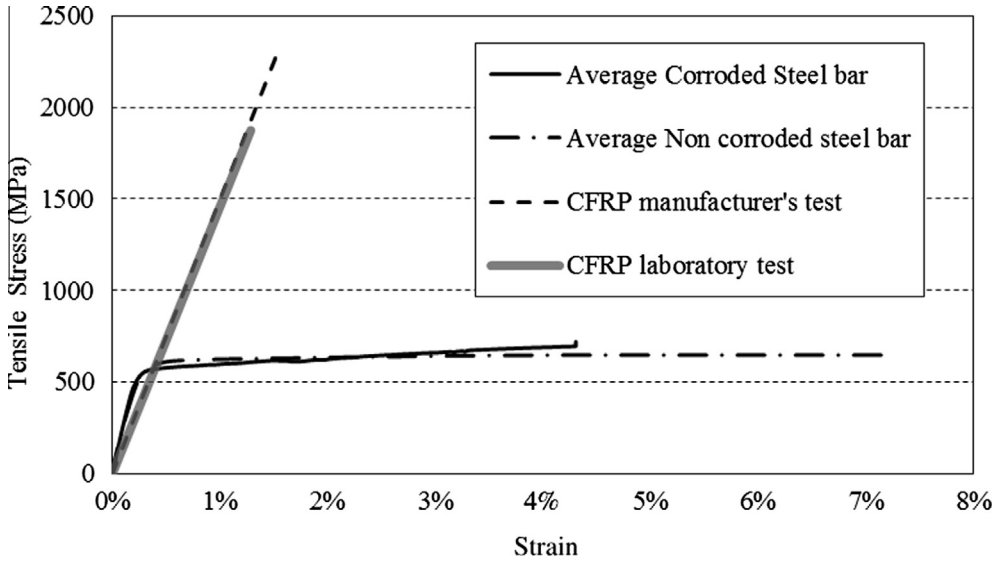

Fig. 3. stress–strain diagrams for steel and CFRP bars.

Table 5
Characteristics of CFRP rods.

Type of test	Ultimate strength (MPa)	Modulus of elasticity (MPa)
Manufacturer's test	2300	150,000
Laboratory test	1875	145,900

Table 6
Filling material properties.

Material	Compressive strength (MPa)	Tensile strength (MPa)	Elastic modulus (MPa)
Epoxy	83	29.5	4900

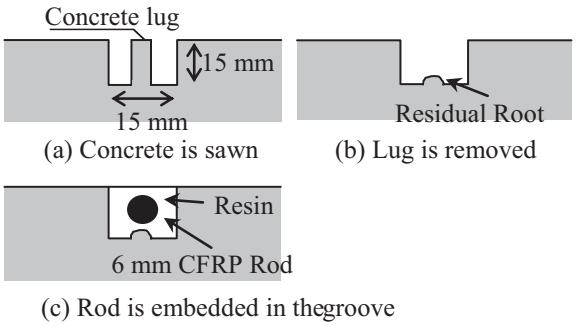

Fig. 4. Installation of CFRP rod in concrete surface.

The remaining concrete lug formed by the sawing was then removed using a hammer and hand chisel so that the lower surface became rough (Fig. 4). The groove was airbrushed to remove dust, debris and fine particles so as to ensure proper bonding between the paste and the concrete. Then, the groove was half filled and the CFRP rod was positioned inside it and pressed lightly. This forced the paste to flow around the CFRP rod. More paste was applied to fill the groove and the surface was levelled. As a result, the CFRP rod was placed in the middle of the cross-section in the tension area. The CFRP rod had a total length of 3000 mm and a diameter of 6 mm, which means that the repair was along the whole length of the beam. The groove was 15 mm deep and 15 mm wide (around 2.5 times the rod diameter) [33]. Previous study was done by Al-Mahmoud et al. [34] showed that FRP below supports and FRP away of the supports did not change the failure mode which was due to the pull-out of the CFRP rod. The two beams were tested one week after installation of the CFRP rod in order to ensure that the filling material reached its full strength.

After the two full span lengths of the corroded beam A1CL3-R and control beam A1T-R had been loaded up to failure, the four end parts (A1CL3-SB, A1CL3-B, A1T-SB and A1T-B) shown in Fig. 5 were extracted of the full span of the two beams. Fig. 6 presents the moment-deflection curves for both full span beams A1CL3-R and A1T-R.

Fig. 7 illustrates the failure of mode for both beams, the corroded A1CL3-R beam which failed due to separation of the concrete cover at the middle of the beam, and the control A1T-R beam which failed due to concrete crushing.

The two left end parts (A1CL3-B and A1T-B) were re-repaired in bending only by replacing the cracked areas of the epoxy paste material with fresh epoxy paste of the same type while the two right end parts (A1CL3-SB and A1T-SB) were re-repaired in bending and in shear using the configuration shown in Fig. 8: four rods were installed 10 cm apart on each side of each end. In order to obtain better repair, the CFRP rods were inclined at 45 degrees so that they would be perpendicular to the shear cracks. The repair plan for all beams is presented in Table 7.

2.4. Instrumentation of beams

In order to verify the anchorage between the longitudinal steel bars and the concrete during the loading process, the slip of the longitudinal steel bars was measured using linear variable differential transducers (LVDT) fixed at either end of each steel bar. One more LVDT was fixed at the mid-span to measure the deflection of the beam as shown in Figs. 9 and 10.

Table 7
Repair plan for all beams.

Beams	Dimensions $h \times b \times L$ mm	Corrosion status	Repair with CFRP NSM rods	
A1CL3-B	280 × 150 × 800	Corroded	Bending	–
A1CL3-SB	280 × 150 × 800	Corroded	Bending	Shear
A1T-B	280 × 150 × 800	Non corroded	Bending	–
A1T-SB	280 × 150 × 800	Non corroded	Bending	Shear

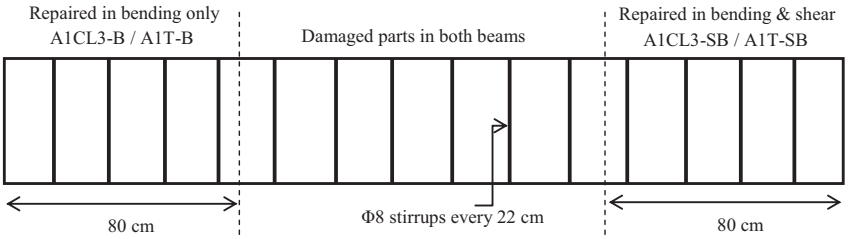

Fig. 5. Parts of corroded and control beam.

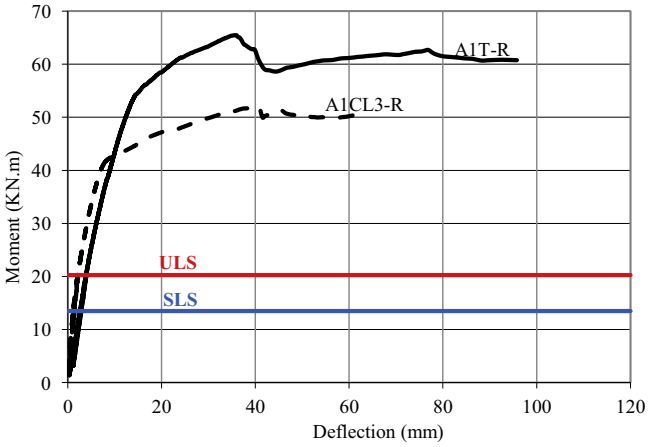

Fig. 6. Moment-deflection curves for A1CL3-R and A1T-R.

As shown in Fig. 9, the LVDT in testing the full span beams (A1CL3 and A1T) was installed at the middle of the beam-span on the same steel support plates as in this case no settlement will take place for both supports while the mid-span LVDT in testing the short beams (A1CL3-B, A1CL3-SB, A1T-B and A1T-SB) was installed on a separate steel plate which takes into account the supports settlement. LVDT at the end of steel bars were fixed on the concrete surface as shown in Fig. 10.

3. Experimental results

3.1. Losses of diameter due to corrosion for tensile steel bars and steel stirrups in corroded beams A1CL3-B and A1CL3-SB

Clark's solution ANSI/ASTM G1-72 was used to remove the corrosion from the surface of the steel reinforcement bars and then the diameter loss of the bars due to corrosion was measured using two different methods: direct measurement with a vernier calliper just after the steel bars had been cleaned and dried, and measurement of the weight loss of the steel bar to calculate the diameter loss. The second method required the critical parts of corroded steel bars to be cut into small pieces 1–2 cm long, which were then weighed to an accuracy of 0.001 g. A reference mass was measured on bars extracted from the control beam. Both methods were used to evaluate the diameter loss of the corroded steel bars as some

(a) A1CL3-R Corroded Beam (b) A1T-R Control Beam

Fig. 7. Modes of failure and damages of two full span beams A1CL3-R and A1T-R.

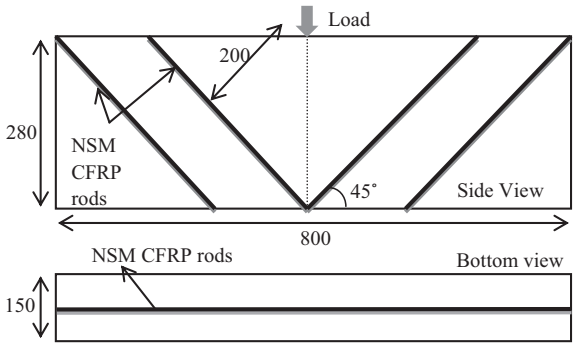

Fig. 8. Shear repair configuration for A1CL3-SB and A1T-SB (Dimensions in mm).

previous papers [35] had shown that the shape of corrosion damage was too complex to be measured only by the vernier calliper.

The maximum diameter loss was found to be 18% at 28 cm away from the mid-span position of A1CL3-B, while 9% diameter loss was found in A1CL3-SB at 20 cm away from mid span. Fig. 11 presents the diameter loss percentage for tensile steel bars at all locations along the two corroded beams.

The steel stirrups were numbered to indicate the part of the beam they came from and their position in that part (the first number represents the part of the beam and the second number represents the number of the stirrup) as shown in Fig. 12.

Fig. 13 shows the locations of corrosion in the steel stirrups and the diameter values. No corrosion was found at stirrups 1–1 and 1–2, the maximum diameter loss found in beam A1CL3-B was 63% at stirrup 1–4 while the maximum loss in A1CL3-SB was 38% at stirrup 3–1.

3.2. Ultimate load capacity and failure modes

Fig. 14 shows the load–deflection curves at the mid-span point for all beams.

The shear repaired control beam A1T-SB failed at 414.6 kN. This was larger than the ultimate load capacity of control beam A1T-B not repaired for shear, which failed at 337.4 kN. The ultimate load capacities of shear repaired corroded beam A1CL3-SB and the non-shear-repaired beam A1CL3-B were close to each other (367.8 kN and 373.3 kN respectively). Fig. 14 also shows that the stiffness of shear-repaired beams A1T-SB and A1CL3-SB was different from that of the non-shear-repaired beams A1T-B and A1CL3-B. The different cracking pattern, shown in Fig. 15, can explain this difference in stiffness. Fig. 14 also presents the load–deflection curves for two similar non-repaired short span beams (75 cm), one control and one corroded A2CL2-A, tested by Dang [36]. Fig. 14 also shows that both the control non-repaired beam tested by Dang [36] and

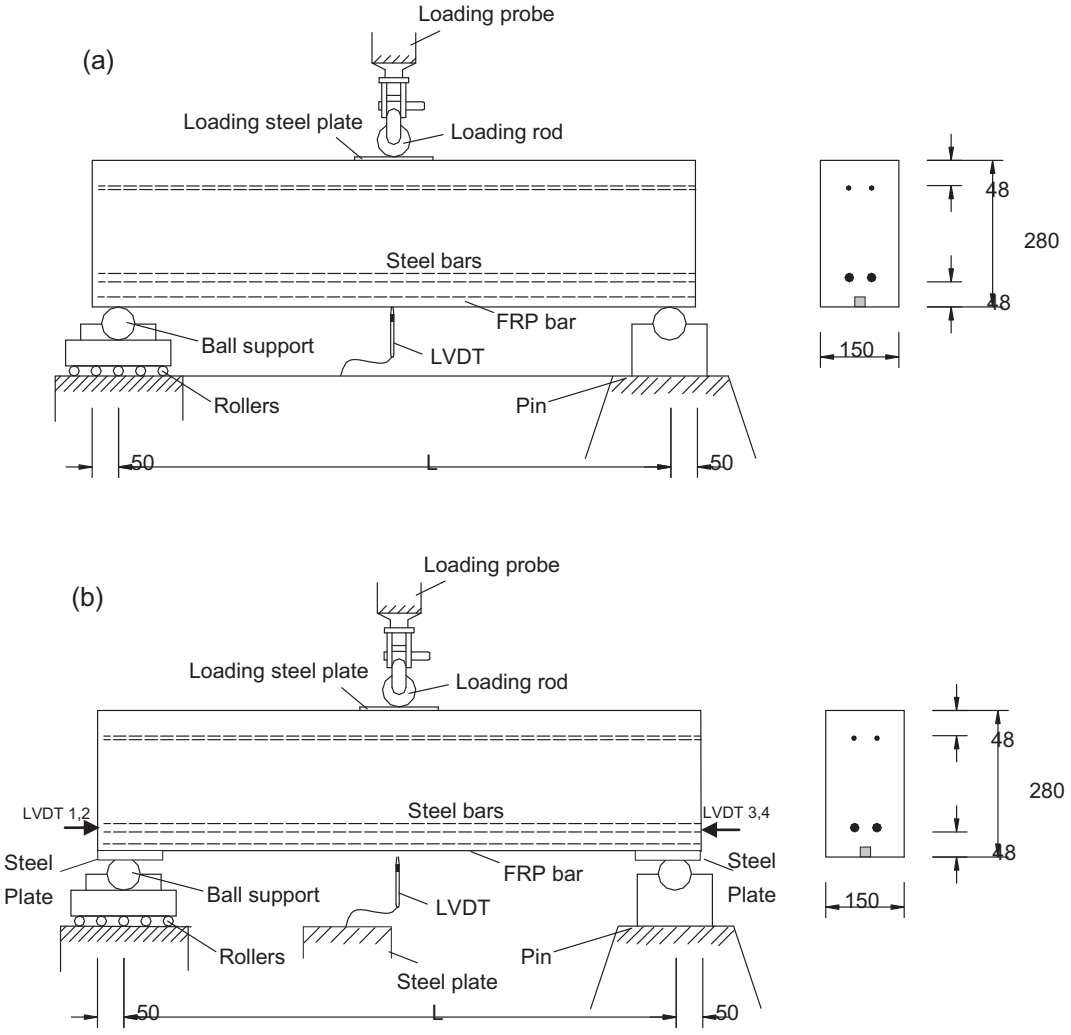

Fig. 9. Beams instrumentation for (a) full span beams and (b) short beams.

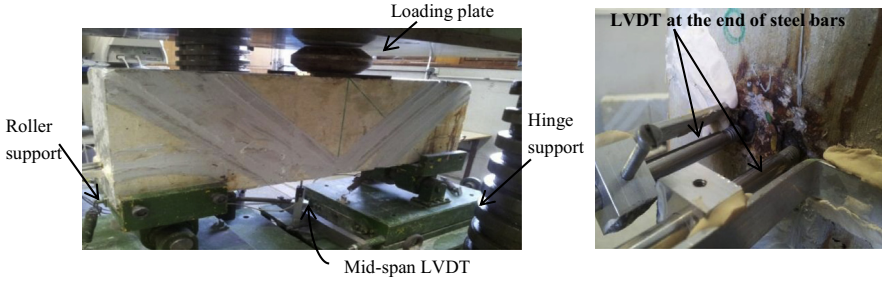

Fig. 10. Short span beams instrumentation.

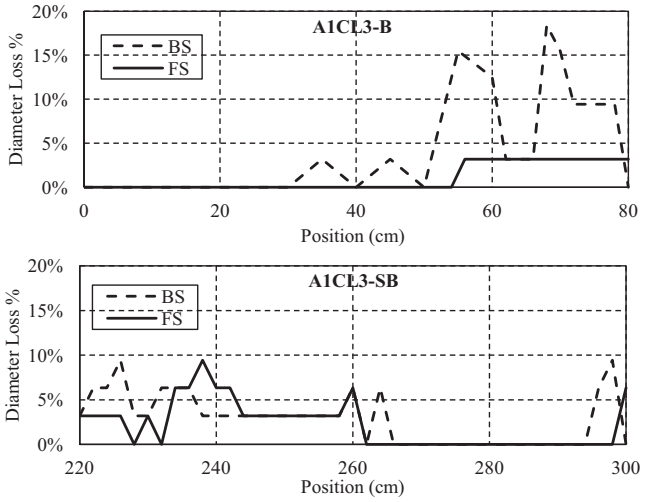

Fig. 11. Diameter loss percentages of longitudinal tensile steel bars.

the beam repaired in bending A1T-B have almost the same yielding capacity which reflects that the strengthening with NSM FRP rod in bending did not increase the anchorage capacity for both beams as they failed with diagonal tension failure with slipping of tensile steel bars.

The same ultimate load capacity values were obtained for both beams A1T-B and A1CL3-B as there was no steel corrosion found at the end of beam A1CL3-B where diagonal crack appears (Fig. 11), the post-yielding deflection difference between both beams can be explained by the difference of the tensile steel bars slipping of both beams (Fig. 18) as in case of A1CL3-B, the maximum slipping was only between 10% and 20% of the maximum slipping of A1T-B.

As shown in Fig. 15, repairing against shear changed the mode of failure for the beams from diagonal tension failure to compression crushing of concrete, the shear repaired control and corroded beams (A1T-SB and A1CL3-SB) failed due to compression crushing of concrete while the non-shear-repaired corroded beam A1CL3-B, failed due to a combination of diagonal tension failure and compression crushing of the concrete. This was not the case for the non-shear-repaired control beam A1T-B, which failed due to diagonal tension failure induced by slipping of the tensile steel bars.

Shear strengthening leads to a change in failure mode from diagonal crack failure close to support due to slipping of re-bars at anchorage, to large flexural crack at mid span followed by concrete crushing. As a result, yielding of tension steel bars which occurred close to support for beams without shear strengthening move to mid-span for shear strengthening beams.

Fig. 16(a) shows the yielding load capacity values for beams non-repaired in shear with NSM FRP rods, all of the beams were failed due to diagonal tension crack failure with the slipping of tensile steel bars, the decrease in yielding capacity for A2CL2-A beam compared with the others refer to the 10% loss in cross section due to corrosion which found in tensile steel bars at the edge of the beam (the same edge of diagonal tension failure) [36], while Fig. 16(b) shows the difference in yielding capacity for the two beams repaired in shear with NSM FRP rods, the difference also happened due to the 6% loss in tensile steel bar diameter (Fig. 11) which meets 12% loss in cross section at mid span.

Diagonal shear failure occurred always on the same side of the short beams whatever the corrosion damage because of the difference in anchorage length between both beam edges. Indeed, Fig. 17 presents the steel layout inside the four beams A1T-B, A1T-SB, A1CL3-B and A1CL3-SB, the load was located at the middle of each beam while the steel geometry is not symmetrical inside the beams as there is 2 cm at the edge of each full beam, the diagonal tension crack failure and the tensile steel bar slip happened in the NC edge as shown in Fig. 15.

3.3. Slip measurements

Fig. 18 shows the slip measured for tensile steel bar ends in all tested beams.

The steel bars started to slip at 170 kN and 150 kN in the non-shear-repaired corroded beam (A1CL3-B) and control beam (A1T-B) respectively, while for beams A2CL3-A and A2CL3-B tested by Khan et al. [12], slipping started at 100 kN and 150 kN respectively.

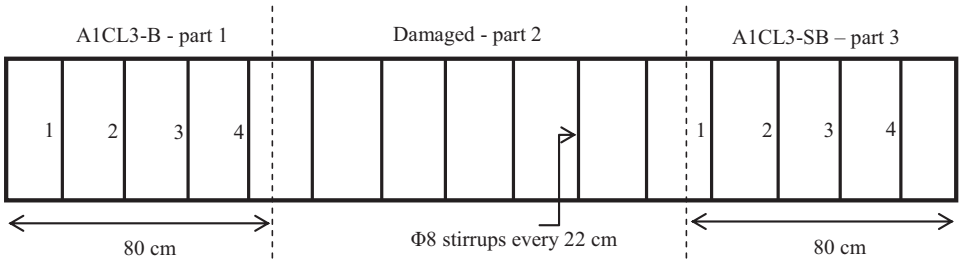

Fig. 12. Parts of corroded beam A1CL3-R.

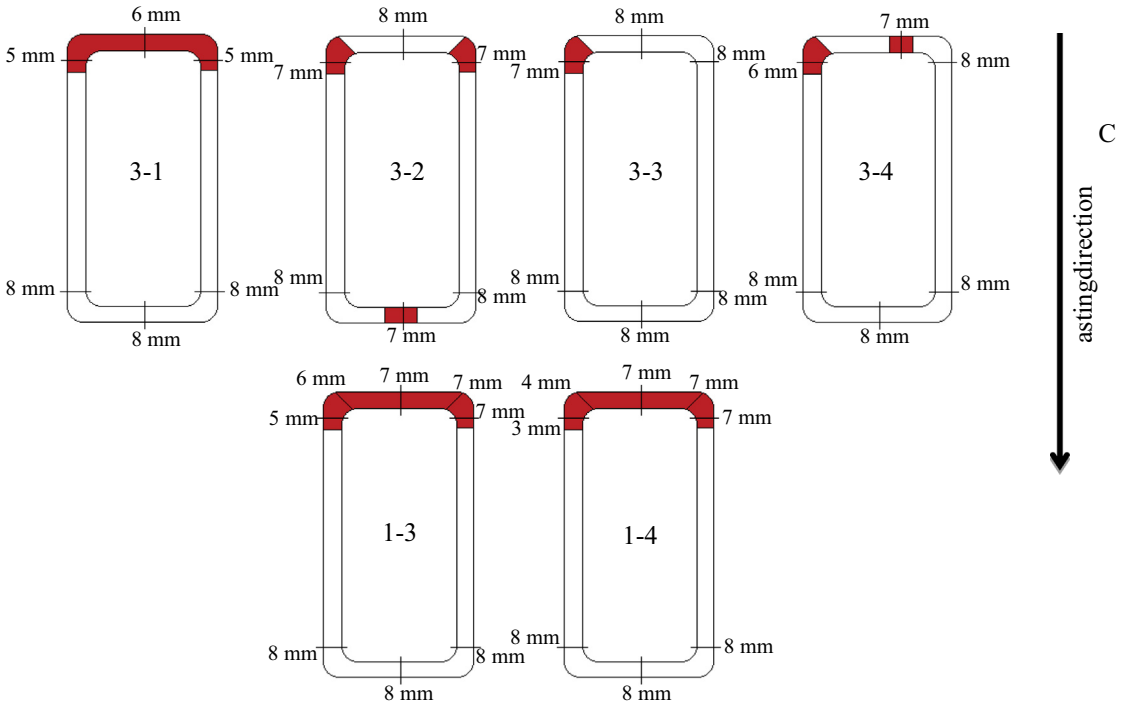

Fig. 13. Corrosion in steel stirrups of corroded beam A1CL3-R.

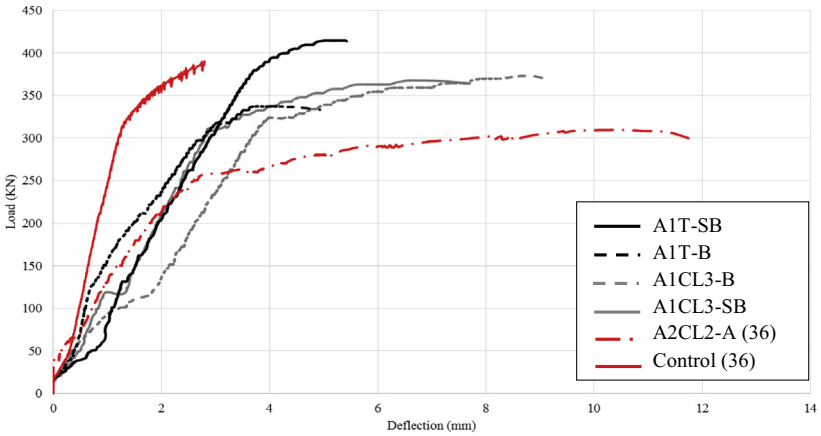

Fig. 14. Load–deflection curves for all beams.

Fig. 18 shows that, without shear repair, slipping of the tensile steel bars was greater in the case of non-corroded beam (A1T-B) than in the case of corroded beam (A1CL3-B), Fig. 18 also shows the slipping of the tensile steel bars for one control beam and one corroded beam A2CL2-A (non-repaired neither in bending nor in shear with NSM) tested by Dang [36]. Moreover, failure of control beam (A1T-B) was a consequence of the re-bar slipping on the support. This result may appear surprising, as it is usually accepted that corrosion reduces the bond stress [37], it must be borne in mind that the natural corrosion process [38] confinement due to both the corroded stirrups [39] and the reactive force on the support modify the bond capacity as shown by Cairns et al. [40]. Moreover, natural corrosion of beam A1CL3-B did not lead to corrosion all around the perimeter of the re-bars and so did not result in the same change in bond strength as the accelerated corrosion induced by impressed current that is usually described in literature.

As shown in Fig. 18, which compares the shear-repaired beams A1T-SB and A1CL3-SB with beams A1T-B and A1CL3-B not repaired in shear and beams not repaired neither in bending nor in shear with NSM Dang [36], it is clear that repairing for shear with NSM CFRP rods significantly increased the anchorage capacity.

3.4. Effect of corrosion

The effect of corrosion on the shear resistance is a complicated area of study due to the variability in failure modes. In this section, the data of maximum corrosion damage was used for comparison in terms of load bearing capacity. Khan et al. [12] tested two beams (A2CL3-A and A2CL3-B) of the same type as those tested in this

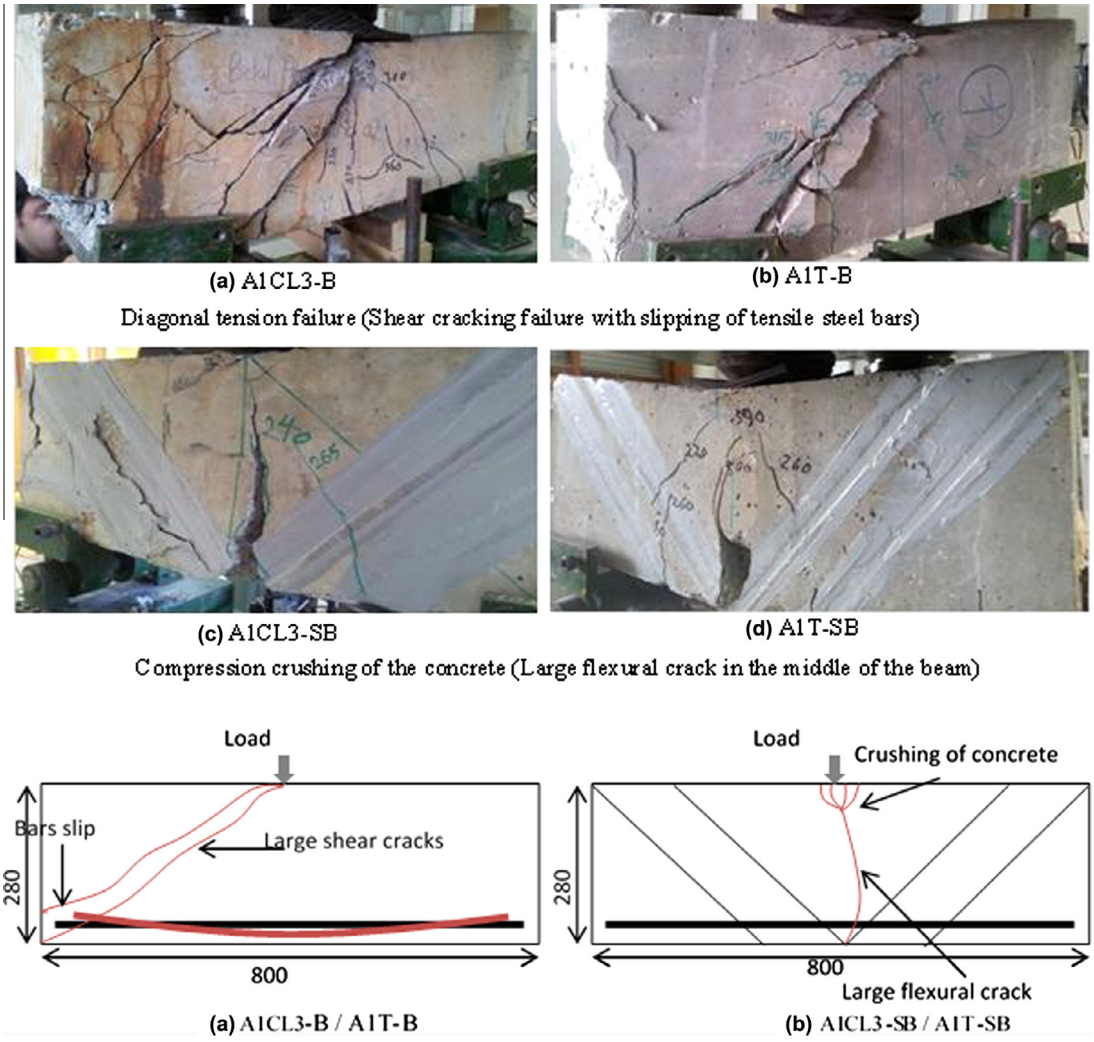

Fig. 15. Failure modes for all beams tested.

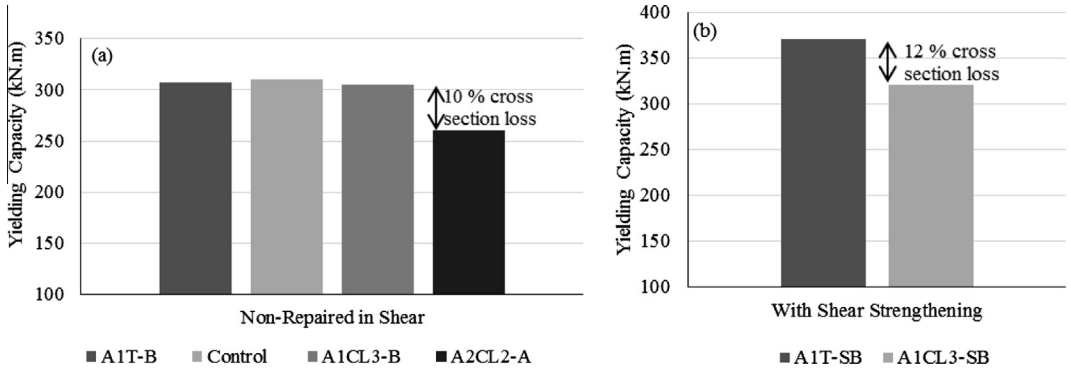

Fig. 16. Yielding capacity values for all beams.

study but which were 1.15 m long without any repair either in bending or in shear. The maximum loss in the cross sectional area of the steel was found to be 25% and 21% in longitudinal tensile steel bars, and 36% and 60% in the steel stirrups for A2CL3-A and A2CL3-B respectively. The re-bar diameter loss was not reflected by a significant change in the ultimate load capacity compared to the control beam (values shown in Table 8). This agrees with the results found here, as the maximum load capacities for corroded beam A1CL3-B and control beam A1T-B were 373.3 kN and 337.4 kN respectively. The maximum diameter loss of longitudinal steel bars was 18% for beam A1CL3-B and 9% for A1CL3-SB. The diameter loss of the longitudinal steel bars at the middle of beam A1CL3-SB was 6%, which corresponds to 12% loss of cross section and matches the theoretical 46.2 kN (0.12×385) loss in the yielding capacity in comparison with A1T-SB. The loss in yielding capacity was found to be 50 kN experimentally, as shown in Fig. 19.

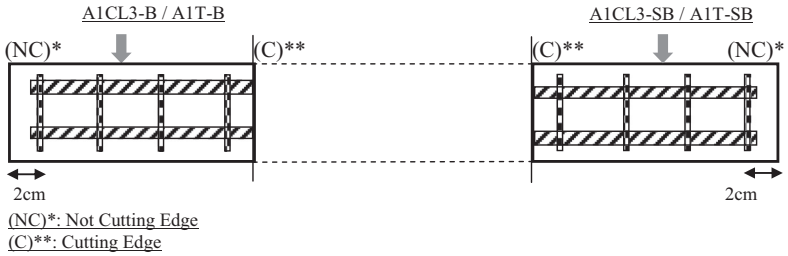

Fig. 17. Steel layouts inside the four beams.

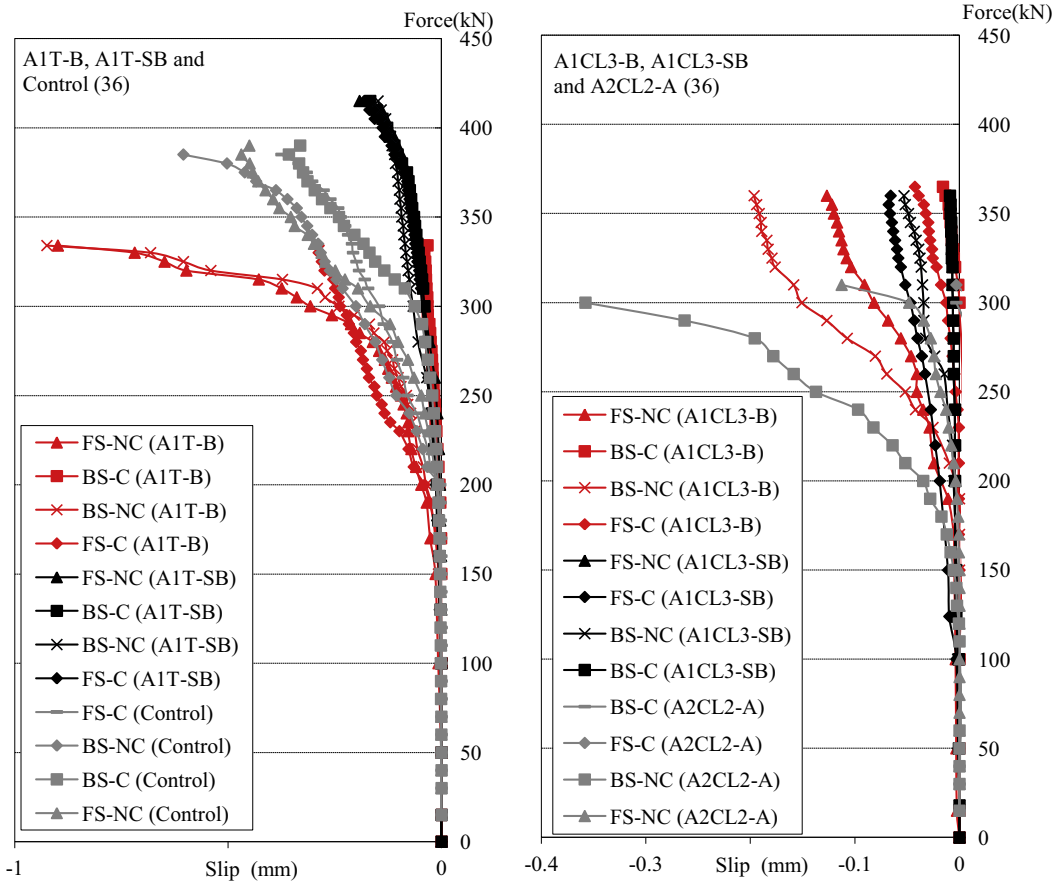

Fig. 18. Slip measurements for all beams.

Table 8
Summary of NSM CFRP repair effect for repaired and non-repaired beams.

Beam	Type of repair	Max. diameter loss in steel bars (%)	Ultimate load (kN)	Failure mode
A1T-B	Bending	0	337	Diagonal tension failure & slip of tensile steel bars
A1T-SB	Bending & shear	0	415	Compression crushing of the concrete
A1CL3-B	Bending	18	373	Diagonal tension failure & slip of tensile steel bars
A1CL3-SB	Bending & shear	9	368	Compression crushing of the concrete
A2T [12]	Non	0	261	Diagonal tension failure
A2CL3A [12]	Non	25	230	Diagonal tension failure
A2CL3B [12]	Non	21	256	Diagonal tension failure

It is also noteworthy that the slipping of the steel bars that occurred in the corroded beam A1CL3-B was on the left side (not corroded) while, on the other side (corroded with 18% of diameter loss), no slip was recorded, which agrees with findings on the control beam A1T-B as a great deal of slip was recorded in that beam despite the fact that it was not corroded. The same result found by Khan et al. [12] who recorded more steel bar slip in the control beam than in the corroded one.

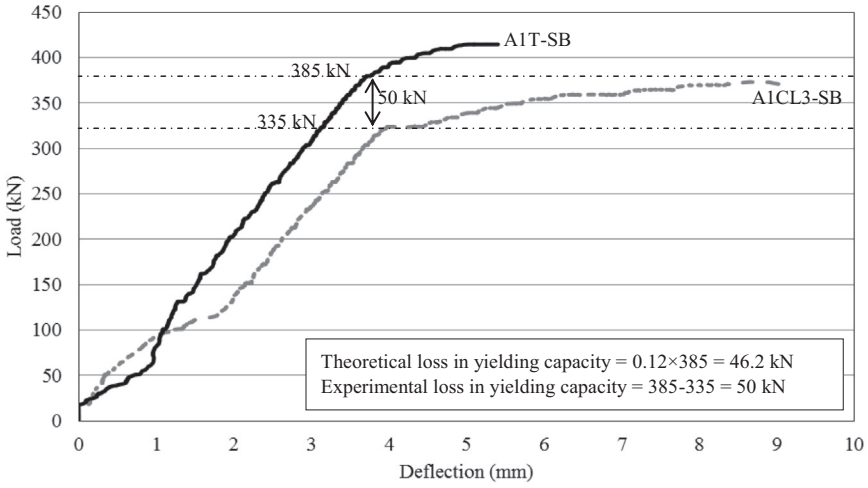

Fig. 19. Effect of corrosion on yielding load capacity of beams repaired in shear.

3.5. Effect of NSM CFRP repair on the ultimate load capacity

A summary of test results for the CFRP repair on tested beams is presented in Tables 8–10. In order to compare the ratio of shear span "*a*" to effective depth "*d*" (*a*/d ratio) for all beams, a dimensionless parameter *k* is introduced; it corresponds to the *a*/*d* ratio divided by the load capacity ratio assuming that for short span beams, the ultimate capacity is proportional to the span.

It is clear that the NSM repair in shear has a crucial effect on the load capacity of RC control beams, as the slip of tensile steel bars was reduced in this case. As shown in Table 9, the non-repaired control beams gave a value of *k* less than 1 in comparison with control beam repaired in shear and bending with NSM (A1T-SB) which denotes the increase percentage in load capacity over the non-repaired control beams tested in [12] and [36]. For corroded beams (Table 10), the shear repair with NSM had no effect on load capacity for *a*/*d* greater than 2.7. On the other hand, there was no marked increase in the load capacity due to repair with NSM for corroded beams which that had *a*/*d* values less than 2, which could be explained by the reduced importance of the bending effect of RC beams as the *a*/*d* values decreased.

3.6. Effect of a/d ratio on the shear strength

Kani [41,42] was one of the first to study the effect of size for slender, deep beams. One important parameter having a crucial effect on the shear strength value is the span to section depth (effective) ratio (*a*/*d*) of the beam, for which Kani [41] found a transitional point of *a*/*d* ratio around 2.5–3. Below this point, the beams developed an arch action and had a considerable reserve of strength beyond the first cracking point. In this paper the *a*/*d* effect was studied for the beams repaired with NSM by plotting the experimental values of shear strength for beams having different values of *a*/*d*, some of which were repaired with NSM in bending and shear, while others were repaired in bending only and the rest were non-repaired beams. The analytical load capacities using the classical bending theory have also been added to the graph as a reference (Fig. 20).

Table 9
Effect of shear repair with NSM for control beams.

Beam	*a*/*d* [(1)]	Ultimate Load (kN)	Load capacity ratio (R1) (4/5)	*a*/*d* ratio (R2) (3/2)	*k*: (R2)/(R1)
A1T-SB	1.4[(2)]	415[(4)]	–	–	–
A2T [12]	2[(3)]	261[(5)]	1.59	1.43	0.90
Control 1 [36]	3.125[(3)]	119.2[(5)]	3.48	2.23	0.64
Control 2 [36]	2.7[(3)]	155[(5)]	2.68	1.93	0.72

Table 10
Effect of shear repair with NSM for corroded beams.

Beam	*a*/*d* [(1)]	Ultimate load (kN)	Load capacity ratio (R1) (4/5)	*a*/*d* ratio (R2) (3/2)	*k*: (R2)/(R1)
A1CL3-SB	1.4[(2)]	368[(4)]	–	–	–
A2CL3A [12]	2[(3)]	230[(5)]	1.60	1.43	0.89
A2CL3B [12]	2[(3)]	256[(5)]	1.44	1.43	0.99
A2CL1-A [36]	3.125[(3)]	110[(5)]	3.35	2.23	0.67
A2CL2-B [36]	2.7[(3)]	120[(5)]	3.07	1.93	0.63
A2CL2-A [36]	1.67[(3)]	310[(5)]	1.19	1.19	1

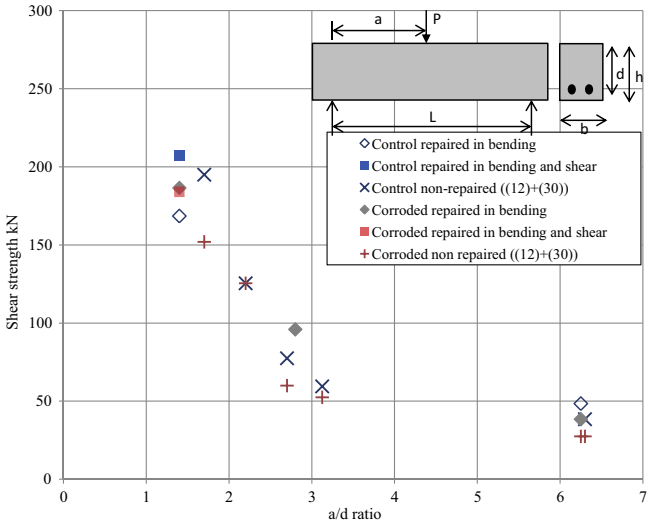

Fig. 20. *a*/*d* ratio effect on the shear strength of beams.

Fig. 20 shows two general trends for the shear strength values; the first trend represent the deep beams (*a*/*d* less than 3) and the second represents the slender beams (*a*/*d* greater than 3). It is clear that the shear strength decreases for increasing *a*/*d* ratios and the reduction in shear strength is steeper than in the slender beams, in agreement with the result found by Higgins and Farrow [43]. The

a/d ratio is considered to be an important parameter for deep beams as the general trend found for such beams is far from the classical bending theory effect. By adding FRP in shear, not only the bonding anchorage but also the yielding capacity of the whole beam was increased. As also shown in Fig. 20, the control beam repaired in shear gave a higher value of shear strength than the non-repaired ones.

Shear resistance mechanism of non-strengthened and non-corroded elements is not totally clarified [44], shear is one of a few areas of research into fundamentals of the behaviour of concrete structures where contention remains amongst researchers. There is a continuing debate between researchers from a structures perspective and those from a materials or fracture mechanics perspective about the mechanisms that enable the force flow through a concrete member and across cracks) and so with corrosion and NSM strengthening, the complexity of the problems will increase significantly.

4. Conclusion

According to the results found in this paper, the following conclusions can be drawn:

1. The failure mode of all non-shear-repaired RC beams (corroded and control) was due to shear cracking while, for shear-repaired beams the failure mode changed to concrete crushing with a large flexural crack at the middle.
2. Corrosion reduced the slip of the tensile steel bars on the support as the pressure induced by the support closed the corrosion induced cracks. As a result, loss of anchorage which was the cause of failure for non-repaired control beams was not involved in the failure of non-repaired corroded beams.
3. Depending on the location of cracks induced by the load during the mechanical testing, the corrosion found in the vicinity of cracks led to a reduction in the yielding capacity of the corroded RC beam.
4. Repairing against shear using NSM FRP rods significantly decreased the maximum slip of the tensile steel bars for control RC beams.
5. No marked effect of shear repair with NSM was recorded on the load capacity of corroded beams having shear span to effective depth ratio values less than 2.
6. Even with reinforcement corrosion and use of repair CFRP rods in both bending and shear, there was still a change in mechanical response in bending for a/d ratios around 2.5–3, which is a transition zone between bending response and shear response.
7. Non-linear numerical models which are able to consider both corrosion damage and strengthening interventions with NSM are required in the future.

References

[1] Schmitt G. Global needs for knowledge dissemination, research, and development in materials deterioration and corrosion control. World Corros Organ NY; 2009.
[2] Andrade C, Alonso C, Garcia D, Rodriguez J. Remaining lifetime of reinforced concrete structures: effect of corrosion on the mechanical properties of the steel. In: Proceedings of the international conference on life prediction of corrodible structures. National Association of Corrosion Engineers, Cambridge, UK, 23–26 September; 1991. p. 12/1–11.
[3] Al-Sulaimani G, Kaleemullah M, Basunbul I Rasheeduzzafar. Influence of corrosion and cracking on bond behaviour and strength of reinforced concrete members. ACI Struct J 1990;87(2):220–31. ASTM G1.
[4] Rodriguez J, Ortega L, Casal J. Load carrying capacity of concrete structures with corroded reinforcement. Constr Build Mater 1997;11(4):239–48.
[5] Chung L, Najm H, Balaguru P. Flexural behavior of concrete slabs with corroded bars. Cem Concr Compos 2008;30(3):184–93.
[6] Azad AK, Ahmad S, Azher SA. Residual strength of corrosion-damaged reinforced concrete beams. ACI Mater J 2007;104(1).
[7] Torres-Acosta AA, Navarro-Gutierrez S, Terán-Guillén J. Residual flexure capacity of corroded reinforced concrete beams. Eng Struct 2007;29(6):1145–52.
[8] Xia J, Jin W, Li L. Shear performance of reinforced concrete beams with corroded stirrups in chloride environment. Corros Sci 2011;53(5):1794–805.
[9] Wang X-H, Li B, Gao X-H, Liu X-L. Shear behaviour of RC beams with corrosion damaged partial length. Mater Struct 2012;45(3):351–79.
[10] Wang X-H, Gao X-H, Li B, Deng B-R. Effect of bond and corrosion within partial length on shear behaviour and load capacity of RC beam. Constr Build Mater 2011;25(4):1812–23.
[11] Zhu W, François R. Effect of corrosion pattern on the ductility of tensile reinforcement extracted from a 26-year-old corroded beam. Adv Concr Constr 2013;1(2):121–37.
[12] Khan I, François R, Castel A. Experimental and analytical study of corroded shear-critical reinforced concrete beams. Mater Struct 2014;47:1467–81.
[13] De Lorenzis L, Nanni A. Shear strengthening of reinforced concrete beams with near-surface mounted fiber-reinforced polymer rods. ACI Struct J 2001;98(1).
[14] Islam AA. Effects of NSM CFRP bars in shear strengthening of concrete members. ASCE; 2009. p. 1–14.
[15] Rizzo A, De Lorenzis L. Behavior and capacity of RC beams strengthened in shear with NSM FRP reinforcement. Constr Build Mater 2009;23(4):1555–67.
[16] Dias SJ, Barros JA. Performance of reinforced concrete T beams strengthened in shear with NSM CFRP laminates. Eng Struct 2010;32(2):373–84.
[17] De Lorenzis L, Nanni A, La Tegola A. Flexural and shear strengthening of reinforced concrete structures with near surface mounted FRP rods; 2000. p. 521–8.
[18] Barros JA, Baghi H, Dias SJ, Ventura-Gouveia A. A FEM-based model to predict the behaviour of RC beams shear strengthened according to the NSM technique. Eng Struct 2013;56:1192–206.
[19] Castel A, François R, Arliguie G. Mechanical behaviour of corroded reinforced concrete beams – part 1: experimental study of corroded beams. Mater Struct 2000;33(9):539–44.
[20] Vidal T, Castel A, François R. Corrosion process and structural performance of a 17 year old reinforced concrete beam stored in chloride environment. Cem Concr Res 2007;37(11):1551–61.
[21] Dang VH, François R. Influence of long-term corrosion in chloride environment on mechanical behaviour of RC beam. Eng Struct 2013;48:558–68.
[22] Zhu W. Effect of corrosion on the mechanical properties of the corroded reinforcement and the residual structural performance of the corroded beams [Ph.D. thesis]. University of Toulouse; 2014.
[23] Zhang RJ, Yang HL, L'Hostis V, Castel A, François R. Characterization of steel/concrete interface for a long-term corroded beam stored in chloride environment. Adv Mater Res 2011;163:3415–20.
[24] Poursaee A, Hansson C. Potential pitfalls in assessing chloride-induced corrosion of steel in concrete. Cem Concr Res 2009;39(5):391–400.
[25] Yuan Y, Ji Y, Shah SP. Comparison of two accelerated corrosion techniques for concrete structures. ACI Struct J 2007;104(3).
[26] Otieno M, Beushausen H, Alexander M. Prediction of corrosion rate in reinforced concrete structures – a critical review and preliminary results. Mater Corros 2012;63(9):777–90.
[27] French regulations for reinforced concrete structures. B.A.E.L.; 1983.
[28] Khan I, François R, Castel A. Structural performance of a 26-year-old corroded reinforced concrete beam. Eur J Environ Civ Eng 2012;16(3–4):440–9.
[29] EN 206-1. European standard, concrete – part 1: specifications, performance, production and conformity. NF EN 206-1; 2004.
[30] EN 12390-2, 3, 5. Essai pour béton durci: confection et conservation des éprouvettes pour essais de résistance, résistance à la compression des éprouvettes et résistance à la flexion des éprouvettes. Bruxelles: IBN; 2000.
[31] Norme Française NF P18-459 March 2010: Porosity and density test.
[32] AL-mahmoud Firas, Castel A, François R, Tourneur C. Effect of surface preconditioning on bond of carbon fibre reinforced polymer rods to concrete. Cem Concr Compos 2007;29(9):677–89.
[33] Al-Mahmoud F, Castel A, François R, Tourneur C, Marchand J, Bissonnette B, et al. Anchorage and tension-stiffening effect between near-surface-mounted fiber reinforced polymer rod and concrete; 2006.
[34] Al-Mahmoud F, Castel A, François R, Tourneur C. Strengthening of RC members with near-surface mounted CFRP rods. Compos Struct 2009;91(2):138–47.
[35] François R, Khan I, Dang VH. Impact of corrosion on mechanical properties of steel embedded in 27-year-old corroded reinforced concrete beams. Mater Struct 2013;46(6):899–910.
[36] Dang VH. Initiation and propagation phases of re-bars corrosion in pre-cracked reinforced concrete exposed to carbonation or chloride environment [Ph.D. thesis]. l'Institut National des Sciences Appliquees de Toulouse, France; 2013.
[37] Almusallam AA. Effect of degree of corrosion on the properties of reinforcing steel bars. Constr Build Mater 2001;15(8):361–8.
[38] Tahershamsi M, Zandi K, Lundgren K, Plos M. Anchorage of naturally corroded bars in reinforced concrete structures. Mag Concr Res 2014;66(14):729–44.
[39] Hanjari KZ, Coronelli D, Lundgren K. Bond capacity of severely corroded bars with corroded stirrups. Mag Concr Res 2011;63(12):953–68.
[40] Cairns J, Plizzari GA, Du Y, Law DW, Franzoni C. Mechanical properties of corrosion-damaged reinforcement. ACI Mater J 2005;102(4).
[41] Basic facts concerning shear failure. ACI; 1966.
[42] Kani G. How safe are our large reinforced concrete beams? ACI; 1967.
[43] Higgins C, Farrow III WC. Tests of reinforced concrete beams with corrosion-damaged stirrups. ACI Struct J 2006;103(1).
[44] fib Bulletin No. 57. Shear and punching shear in RC and FRC elements; 2010. 268 p.